



Chinese Society of Aeronautics and Astronautics
& Beihang University

Chinese Journal of Aeronautics

cja@buaa.edu.cn
www.sciencedirect.com



Advanced optimization of gas turbine aero-engine transient performance using linkage-learning genetic algorithm: Part II, optimization in flight mission and controller gains correlation development

Yinfeng LIU^a, Soheil JAFARI^{b,*}, Theoklis NIKOLAIDIS^b

^a Aero Engine Test Department of Hunan Aviation Powerplant Research Institute, AECC, Zhuzhou 412002, China

^b Centre for Propulsion Engineering, School of Aerospace Transport and Manufacturing (SATM), Cranfield University, Cranfield MK43 0AL, UK

Received 3 May 2020; revised 26 July 2020; accepted 26 July 2020

Available online 15 August 2020

KEYWORDS

Aeroengine control;
Control optimization;
Flight condition;
Flight mission simulation;
GA;
GTE;
LLGA;
Min-Max controller;
Robustness

Abstract Part I has illustrated the procedures to apply the Linkage Learning Genetic Algorithm (LLGA) in Gas Turbine Engine (GTE) controller gains tuning and generated the optimization results for runway conditions from idle to takeoff. However, the total pressure and temperature of the engine inlet vary as the changing of altitude and Mach number, which would lead to the variation in fuel flow supply regulation. As a result, the optimized gains in runway might not be suitable for other flight conditions. In order to maintain the optimal control performance, the GTE controller gains should be adjusted according to the flight conditions. This paper extends the application of the LLGA method to other flight conditions and then simulates a complete flight mission with different gains and weather condition configurations. For this purpose, the control parameters in the Simulink model of the GTE controller are first corrected by the weather condition in altitude. Then, a typical flight mission is defined and divided into different flight segments based on the altitude and Mach number configuration. One representative point is selected from each segment as the datum point for optimization process. After this step, the LLGA method is used to find the best gains combinations for different flight conditions and the differences in optimization effects for different flight conditions are analyzed subsequently. The simulation results show that the optimization effect of the control performance of each flight condition is dependent on the value of $\sqrt{0.5}$

* Corresponding author.

E-mail address: S.Jafari@Cranfield.ac.uk (S. JAFARI).

Peer review under responsibility of Editorial Committee of CJA.



Production and hosting by Elsevier

<https://doi.org/10.1016/j.cja.2020.07.037>

1000-9361 © 2020 Chinese Society of Aeronautics and Astronautics. Production and hosting by Elsevier Ltd.

This is an open access article under the CC BY-NC-ND license (<http://creativecommons.org/licenses/by-nc-nd/4.0/>).

and the optimal K_{pla} in some flight conditions is approximately equal to $\sqrt{0.8}$ times of the K_{pla} value in sea level standard condition. Finally, the complete flight mission is simulated with different gains and weather condition configurations. The simulation results show that the engine performance has been greatly improved after optimization by LLGA in the transient state and the high altitude conditions. In other steady states, the optimization effect is not very obvious.

© 2020 Chinese Society of Aeronautics and Astronautics. Production and hosting by Elsevier Ltd. This is an open access article under the CC BY-NC-ND license (<http://creativecommons.org/licenses/by-nc-nd/4.0/>).

1. Introduction

When an aircraft flies in the sky, the total pressure and temperature of the engine inlet vary as the changing of altitude and Mach number. This will lead to the variation in fuel flow supply regulation.¹ As a result, the GTE controller gains which work well in Sea Level Standard (SLS) condition may not be suitable for other flight conditions. In order to maintain the good control performance, the GTE controller gains should be adjusted according to the weather condition during the flight mission. Many Meta-heuristic Global Optimization (MGO) algorithms have been proposed and applied in GTE controller optimization problems, including Particle Swarm Optimization (PSO), Ant Colony Optimization (ACO), Invasive Weed Optimization (IWO), and Bee Colony Optimization (BCO).²⁻⁵ However, most of these studies only focus on the controller optimization in SLS condition and the influence of the weather condition exerted on the optimization effect is rarely studied.

The Min-Max controller has been widely used in the industrial control domain and many researches about its applications in aero engine controller were also published.² The fuzzy theory is regarded as one potential methodology to optimize the control performance or tracking performance. Many different T-S fuzzy norms are applied in the Min-Max controller to improve the control performance.⁶ The nonfragile H_∞ filter design method is applied for continuous-time T-S fuzzy systems in⁷ in which the designed filter is assumed to have two types of multiplicative gain variations. The fuzzy adaptive control strategy is also used to solve the asymptotic tracking control problem of a class of uncertain switched nonlinear systems in⁸ where a novel discontinuous controller with dynamic feedback compensator is designed. The nature and characteristics of non-linear switching systems are well-studies in the literature from different points of view including performance and modelling,^{9,10} control strategy design and analysis,^{11,12,13} implementation considerations,^{14,15,16} stabilization,^{17,18} and stability analysis.^{19,20,21} However, most of the papers in gas turbine aero-engines applications treat the Min-Max controller (or other fuzzy norms) as a black box and do not analyze the detail working process inside.^{3,5,6} As a result, sometimes it is not known that which transient loops are activated and which constraint is the dominant limitation during the control process, especially for the transient process. But this detail information is very important to help the designers to analyze the reasons for fluctuation and deviation of the engine performance and guide the direction of improving the control performance.

In part I, a new LLGA method was proposed for GTE controller gains tuning problem and applied in runway condition from idle to takeoff. In this paper, the influence of flight con-

ditions including altitude and Mach number will be considered in the controller performance and then the LLGA method will be extended to GTE controller optimization in different flight conditions. As a result, by adopting different optimized controller gains according to the changing of flight conditions during the whole flight mission, better control performance is expected to be achieved than applying the constant gain values in different flight conditions. For this purpose, the principle to correct the control parameters by weather condition is first presented. Then a classical flight mission is defined and the typical operational points are selected to characterize different flight segments in the flight mission. After this, the LLGA method is used to optimize the controller gains for different flight conditions. The simulation results are analyzed from the aspects of weather condition, working process of the Min-Max selection and the robustness of the GTE controller. Moreover, the complete flight mission simulation is implemented with the GTE controller configured with different gains and weather condition combinations. However, the flight condition changes continuously during the whole flight mission while the optimization controller gains are acquired only based on the representative condition points. This will make the engine performance during the flight condition to be a little different from the simulation results in separate flight conditions, which will also be illustrated in this paper. Finally, the flight mission simulations are implemented with three different control parameter configurations. The simulation results are analyzed and the detail working processes within the Min-Max controller during the flight mission are illustrated. In addition, the control performances of different control parameter configurations are compared to confirm the effectiveness of the proposed methodology to optimize the performance of the engine and controller as a closed-loop system.

2. Control parameters correction

In order to simulate the flight conditions, the altitude and Mach number will be taken into consideration and the rotational speed and fuel flow will be corrected by weather conditions. Therefore, weather condition block is added into the GTE controller model as shown in Fig. 1.

In the SLS, the ambient temperature and pressure are set as 288.15 K and 101325 Pa. The ambient temperature t_H and pressure p_H at altitude H can be calculated by utilizing Eqs. (1) and (2).¹

$$t_H = -0.00657H + 288.15 \quad (1)$$

$$p_H = -8.6462 \times 10^{-9}H^3 + 0.000522H^2 - 11.863H + 101325 \quad (2)$$

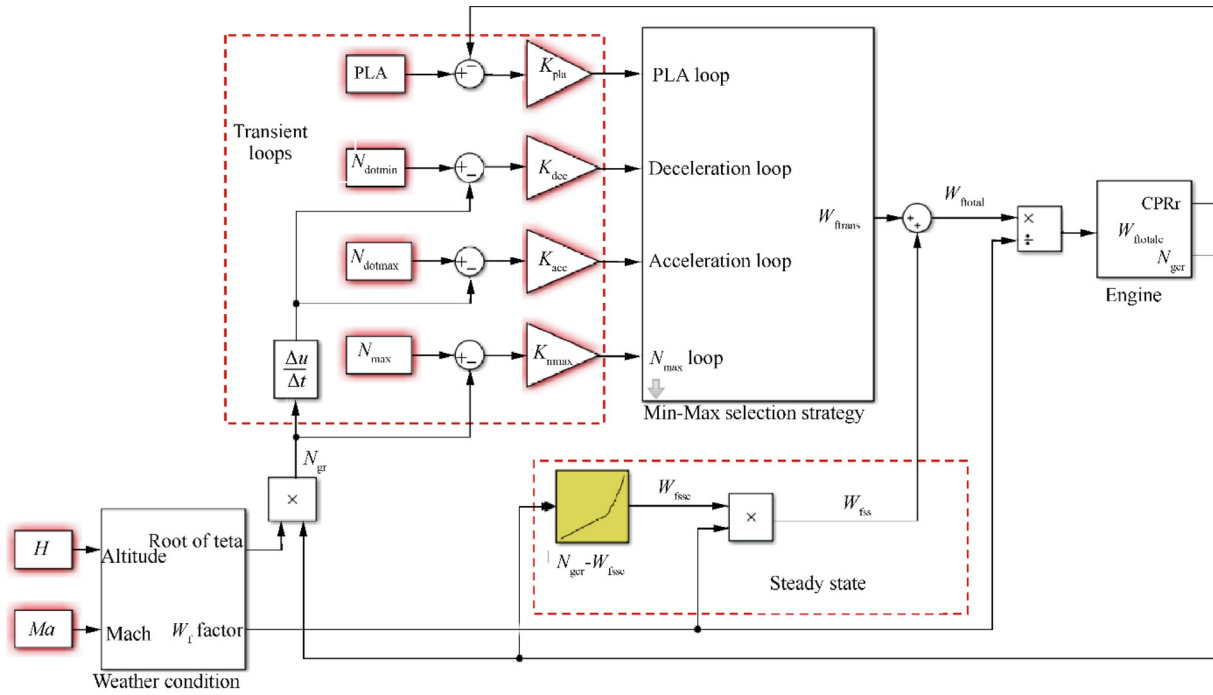


Fig. 1 Schematic of aero-engine fuel controller structure.

Considering the flight Mach number, the total temperature T_H and total pressure P_H of the engine inlet at altitude H and Mach number Ma can be calculated by Eqs. (3) and (4).¹

$$T_H = (1 + \frac{\gamma - 1}{2} Ma^2) t_H \quad (3)$$

$$P_H = \left(1 + \frac{\gamma - 1}{2} Ma^2\right)^{\frac{\gamma}{\gamma - 1}} p_H \quad (4)$$

where γ is the ratio of specific heats and has the constant value of 1.4.

Then non-dimensional temperature θ and pressure δ are calculated by Eqs. (5) and (6).

$$\theta = T_H / 288.15 \quad (5)$$

$$\delta = P_H / 101325 \quad (6)$$

In the limitation loops, the safety concern is evaluated by the physical rotational speed and physical acceleration or deceleration, so the relative corrected rotational speed under SLS, i.e. N_{gr} , should be converted into the relative physical rotational speed N_{gr} before entering the limitation loops as depicted in Eq. (7). As a result, the output of Min-Max selection is the physical transient fuel flow W_{trans} . The corrected steady state fuel flow W_{fssc} is calculated through interpolation method from the fuel- N_{gr} schedule. In order to keep consistent with the transient fuel flow, the output fuel flow from the steady state control loop should also be converted into physical fuel flow W_{fss} by Eq. (8).¹ Before entering the engine, the physical total fuel flow W_{total} should be corrected to W_{totalc} under SLS by Eq. (9). After these steps, the work of building the GTE controller is finished.

$$N_{gr} = \sqrt{\theta} \cdot N_{grc} \quad (7)$$

$$W_{fss} = \sqrt{\theta} \cdot \delta \cdot W_{fssc} \quad (8)$$

$$W_{totalc} = W_{total} / (\sqrt{\theta} \cdot \delta) \quad (9)$$

3. Description of the flight mission and definition of the flight conditions

Fig. 2 shows the altitude and Mach number curves during a typical flight mission. Based on the altitude & Mach number configurations, the flight mission is divided into ten segments which are specified in Appendix. The altitudes of three climb segments are 0–1524 m, 1524–7620 m and 7620–11100 m respectively. The equivalent air speed during the altitude range 457.2–7620 m is around 128.5 m/s (250 kts). For the sake of simplicity, one representative point is selected from each segment and depicted in Table 1. In Section 4, the LLGA method will be applied on GTE controller gains tuning in different

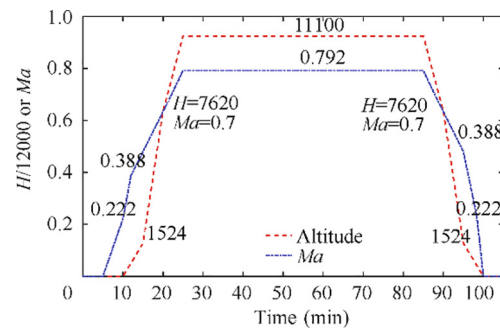


Fig. 2 Altitude and Mach number changing during flight mission.

Table 1 Representative weather conditions for different flight mission segments.

Parameter	Ground idle	Take-off	BOC	Climb	TOC	Cruise	Approach
Height (m)	0	0	457.2	6096	10000	11100	457.2
Ma	0	0.222	0.388	0.589	0.78	0.792	0.233
$\sqrt{\theta}$	1	1.005	1.01	0.9596	0.9306	0.9169	1
δ	1	1.035	1.051	0.5818	0.3912	0.3349	0.9842
$\sqrt{\theta} \cdot \delta$	1	1.04	1.061	0.5582	0.364	0.307	0.9843

Notes: BOC—begin of climb; TOC—top of climb; Begin of descent (BOD) and decent have the same weather conditions as TOC and climb respectively.

flight conditions and the genetic process parameters are the same as part I. The optimized engine control performance will be compared with that of initial controller gains as shown in Table 2. In order to keep the consistency, the PLA command in each simulation scenario will be the same as part I which is shown in Fig. 3. In this figure, the PLA experiences a step increase from 0.6 to 1.0 at $t = 15$ s and a step decrease from 1.0 to 0.7 at $t = 30$ s. This PLA command is used to simulate the sudden change in the input command to the controller as the worst case scenario. Moreover, the definition of the objective function for control performance is also the same as part I which is shown in Eq. (10).

$$J(\text{gains}) = 0.5RT + 0.5FC + 1/6(P_1 + P_2 + P_3 + P_4 + P_5 + P_6) \quad (10)$$

where RT is the normalized response time; FC is the normalized fuel consumption; P_1 is the penalty for oscillation during 0–15 s; P_2 is the penalty for oscillation during 30–45 s; P_3 is the penalty for the error between CPR and PLA; P_4 is the penalty for overspeed; P_5 is the penalty for over acceleration; P_6 is the penalty for over deceleration. The specific definition of each item has been illustrated in part I.

4. Optimization results for different flight conditions

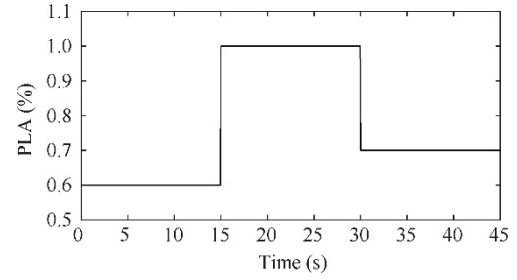
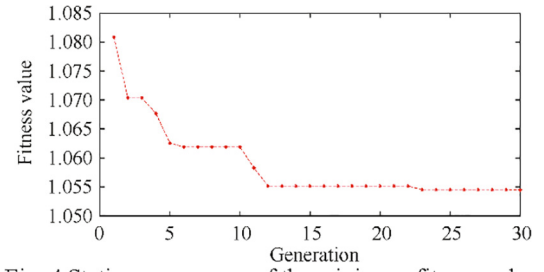
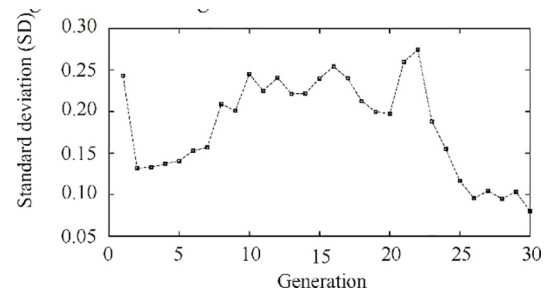
4.1. Take-off ($H = 0$, $Ma = 0.222$)

In the take-off condition, the aircraft is on the ground while the flight speed is accelerated, and the aero-engine works under the maximum power/thrust setting. Apply LLGA on controller gains tuning, then the fitness value convergence is shown in Fig. 4. In the figure, the minimum fitness value is already very low at the first generation and it only decreases by 2.3% during the next 29 generations. This verifies the fact that the minimum fitness value is reduced after BBs detection.

The standard deviation of the fitness value is shown in Fig. 5. The standard deviation has a great decrease in the first 2 generations, then it maintains at a relative high level during the generations of 3–22 and finally experiences an obvious reduction in the last 8 generations. This phenomenon is very

Table 2 Initial gains of GTE controller.³

Parameter	K_{pla}	K_{Nmax}	K_{acc}	K_{dec}
Value	1.7	3	−0.01	5

**Fig. 3** Variation of PLA value for simulation.**Fig. 4** Static convergence of the minimum fitness value.**Fig. 5** Standard deviation of the fitness value at each generation.

similar to the scenario of ground idle and the reason for this has been illustrated in part I.

The final optimization results are depicted in Table 3. Simulate the GTE controller model with the optimized gains and the initial gains respectively, then get the engine performance as shown in Table 4 and Fig. 6. The fitness value is reduced from 1.2029 to 1.0545 after optimization. The RT is reduced by 14.6% while the FC almost remains the same. As for the penalty items, the fluctuation (P_1 , P_2) and the tracking error

(P_3) are greatly reduced, while the maximum acceleration and deceleration value (P_5 , P_6) have some increase. Overall, the benefits brought in by the optimization greatly outweighs the side effects. In addition, the tracking error in this flight condition is caused by the limitation on physical rotational speed. As $\sqrt{\theta}$ ($=1.005$) is larger than 1 in take-off, the N_{gr} should be lower than 1 to make sure that N_{gr} would not exceed the speed limitation. Therefore, the CPR_r also cannot reach the value 1.

The N_{gr} derivative is shown in Fig. 7. In the figure, both the N_{gr} derivative before and after optimization have not exceeded the safe bounds. Moreover, the optimized controller has used the safety margins to improve the engine performance.

4.2. Begin of climb ($H = 457.2$, $Ma = 0.388$)

During the climb part of a flight condition, the aircraft rises from altitude of 0 m to 11,100 m and the Mach number increases from 0.222 Ma to 0.792 Ma . As a result, the GTE inlet total temperature and pressure change a lot during the climb process. In order to ensure the reliability of the optimized controller gains, the climb process is divided into three scenarios, i.e. begin of climb (BOC), climb and top of climb (TOC). The gains tuning of these three flight conditions are studied in Sections 4.2, 4.3 and 4.4 respectively.

In ground idle and take-off, the best fitness values are found in the 28th and the 30th generation respectively. In order to verify whether the fitness value would continue to decrease beyond the 30th generation, the iteration generation in climb is set to be 40. Apply LLGA on controller gains tuning, then the fitness value convergence is shown in Fig. 8. During the whole evaluation process, the minimum fitness value decreases by 3.3% and reaches the bottom at the 26th generation which means that 30 generations are large enough for sufficient convergence. The standard deviation of the fitness value is shown in Fig. 9. It increases in the first 7 generations, then it maintains at a relative high level during the generations of 8–27 and finally experiences an obvious reduction during the generations of 28–35.

The final optimization results are depicted in Table 5. Simulate the GTE controller model with the optimized gains and the initial gains respectively, then get the engine performance as shown in Table 6 and Fig. 10. The fitness value is reduced from 1.5940 to 1.1229 after optimization. The main improvement after optimization is the RT which is reduced by 46.1% while the FC increases by only 0.48%. As the tracking requirement for CPR at PLA = 1 is $CPR_r \geq 0.985$ which cannot be satisfied with the initial gains, thus the RT value with initial gains is very large. As for the penalty items, the fluctuation (P_1 , P_2) and the maximum tracking error (P_3) are greatly reduced; the maximum acceleration and deceleration values (P_5 , P_6) have some increase. Overall, the benefits brought in by the optimization greatly outweighs the side effects. In addition, the tracking error in this flight condition is caused by the

large $\sqrt{\theta}$ value ($=1.005$) which has been illustrated in Section 4.1.

The N_{gr} derivative is shown in Fig. 11. In the figure, both the N_{gr} derivative before and after optimization have not exceeded the safe bounds. Moreover, the optimized controller has used the safety margins to improve the engine performance.

4.3. Climb ($H = 6096$, $Ma = 0.589$)

Climb is the middle part of the rise phase of a flight mission, and its representative condition point is $H = 6096$, $Ma = 0.589$. Set this weather condition in the GTE controller model and apply LLGA on controller gains tuning, then the fitness value convergence is shown in Fig. 12. In the figure, the minimum fitness value is already very low at the first generation and it only decreases by 0.76% during the next 29 generations. Fig. 13 shows the standard deviation of the fitness value at each generation. In this figure, the standard deviation of the fitness value has a dramatic decrease at the first three generations and then maintains at a relative low level during the following generations except for the 23th and 24th generations. The high standard deviations in these two generations are caused by the mutation operator which generates some individuals of high fitness values.

The final optimization results are depicted in Table 7. Simulate the GTE controller model with the optimized gains and the initial gains respectively, then the comparison between the controller performance before and after optimized is depicted in Table 8. The fitness value is greatly reduced from 1.2381 to 0.7990 after optimization. Almost all the items in the objective function are greatly improved after optimization except for RT.

The engine performance with initial gains is shown in Fig. 14. In this figure, the CPR and N_{gr} fluctuates dramatically especially at the PLA settings of 0.6 and 0.7. Moreover, the short response time of initial controller is achieved at the expense of inducing more tracking error and fluctuation. Undoubtedly, the initial gains are unacceptable in the flight condition of climb. The normalized acceleration/deceleration is shown in Fig. 15 and the maximum acceleration has exceeded the surge bound.

The engine performance after controller optimization is shown in Fig. 16. In the figure, the CPR can track with the PLA well while the N_{gr} cannot reach 1. This is because $\sqrt{\theta} < 1$ and N_{gr} will be lower than 1 when $N_{gr} = 1$. The normalized acceleration/deceleration is shown in Fig. 17 and it stays within the safe zone during the whole simulation time.

4.4. Top of climb ($H = 10000$, $Ma = 0.78$)

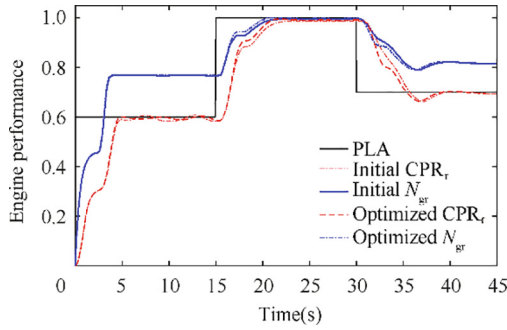
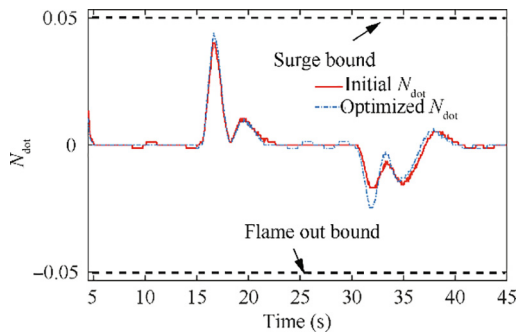
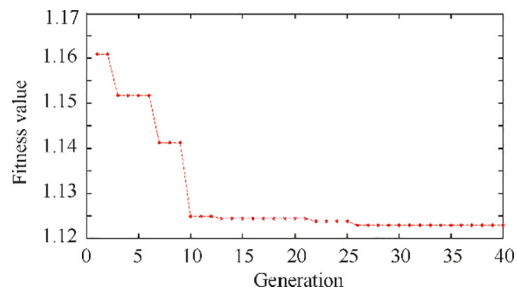
TOC is the third part of the rise phase of a flight mission, and its typical condition point is $H = 10000$, $Ma = 0.78$. Set this weather condition in the GTE controller model and apply

Table 3 Optimized controller parameters.

Parameter	K_{pla}	K_{Nmax}	K_{acc}	K_{dec}	Fitness	Optimization time
Optimized results	1.8307	4.9295	−0.0302	8.2035	1.0545	2498 s

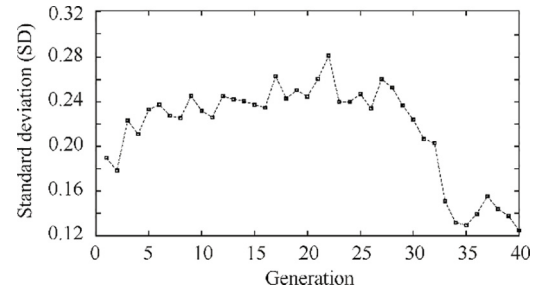
Table 4 Performance and penalty function values before and after optimization.

Parameter	RT	FC	P_1	P_2	P_3	P_4	P_5	P_6	Fitness
Initial	1.0567	1.0054	0.1775	0.1961	0.5882	0	0.0696	0	1.2029
Optimized	0.9027	1.0073	0.1024	0.1945	0.1961	0	0.0813	0.0229	1.0545

**Fig. 6** Engine performance before and after optimization.**Fig. 7** Derivative of engine rotor speed before and after optimization.**Fig. 8** Static convergence of the minimum fitness value.

LLGA on controller gains tuning, then the fitness value convergence is shown in Fig. 18. In the figure, the minimum fitness value decreases by 1% during 30 generations. Fig. 19 shows the standard deviation of the fitness value at each generation. In this figure, the standard deviation reduces a lot as the generation increases, especially for the first four generations.

The final optimization results are depicted in Table 9. Simulate the GTE controller model with the optimized gains and

**Fig. 9** Standard deviation of the fitness value at each generation.

the initial gains respectively, then the comparison between the controller performance before and after optimized is depicted in Table 10. The fitness value is reduced from 3.7445 to 0.7089 after optimization. Almost all the items in the objective function are greatly improved after optimization except for RT.

The engine performance with initial gains is shown in Fig. 20. In this figure, the CPR and N_{gr} fluctuates dramatically and follow the rule that the lower the PLA setting is, the more dramatical fluctuation they have. Moreover, the short response time of initial controller is achieved at the expense of inducing more fluctuation, more tracking error and overspeed. In addition, the CPR has deviated from PLA when PLA = 0.6. Undoubtedly, the initial gains are unacceptable in TOC. The normalized acceleration/deceleration is shown in Fig. 21 and the maximum acceleration/deceleration has exceeded both the surge bound and the flame out bound.

The engine performance after controller optimization is shown in Fig. 22. In the figure, the CPR can track with the PLA well while the N_{gr} cannot reach 1. The reason for this has been illustrated in Section 4.3. The normalized acceleration/deceleration is shown in Fig. 23 and it stays within the safe zone during the whole simulation time.

4.5. Cruise ($H = 11100$, $Ma = 0.792$)

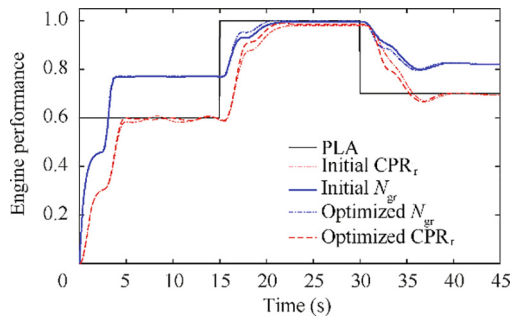
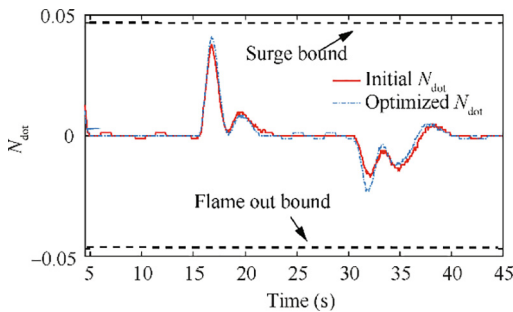
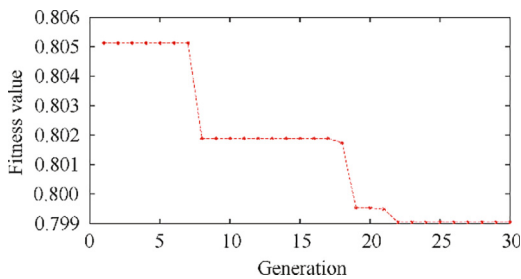
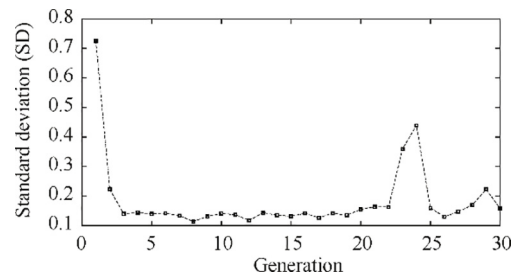
Cruise is the main part of a whole flight mission. In this condition, the aircraft flies in the highest altitude and highest Mach number and the representative condition point is $H = 11100$, $Ma = 0.92$. Set this weather condition in the GTE controller model and apply LLGA on controller gains tuning, then the fitness value convergence is shown in Fig. 24. In the figure, the minimum fitness value decreases by 2.5% during 30 generations. Fig. 25 shows the standard deviation of the fitness value at each generation. In this figure, the standard deviation reduces a lot as the generation increases, especially for the first three generations.

Table 5 Optimized controller parameters.

Parameter	K_{pla}	$K_{N_{max}}$	K_{acc}	K_{dec}	Fitness	Optimization time
Optimized results	1.8454	4.9452	-0.0496	7.9746	1.1229	3321 s

Table 6 Performance and penalty function values before and after optimization.

Parameter	RT	FC	P_1	P_2	P_3	P_4	P_5	P_6	Fitness
Initial	1.6993	1.0173	0.1719	0.1886	0.9804	0	0.0696	0.0035	1.5940
Optimized	0.9167	1.0222	0.0504	0.1780	0.5882	0	0.0813	0.0229	1.1229

**Fig. 10** Engine performance before and after optimization.**Fig. 11** Derivative of engine rotor speed before and after optimization.**Fig. 12** Static convergence of the minimum fitness value.**Fig. 13** Standard deviation of the fitness value at each generation.

The final optimization results are depicted in Table 11. Simulate the GTE controller model with the optimized gains and the initial gains respectively, then the comparison between the controller performance before and after optimized is depicted in Table 12. The fitness value is reduced from 7.2427 to 0.7061 after optimization. Almost all the items in the objective function are greatly improved after optimization except for RT.

The engine performance with initial gains is shown in Fig. 26. In this figure, the CPR and N_{gr} fluctuate dramatically and follow the rule that the lower the PLA setting is, the more dramatical fluctuation they have. Moreover, the short response time of initial controller is achieved at the expense of inducing more fluctuation, more tracking error and overspeed. In addition, the CPR has deviated from PLA during the whole simulation time. Undoubtedly, the initial gains are unacceptable in cruise. The normalized acceleration/deceleration is shown in Fig. 27 and the maximum acceleration/deceleration has exceeded both the surge bound and the flame out bound.

The engine performance after controller optimization is shown in Fig. 28. In the figure, the CPR can track with the PLA well while the N_{gr} cannot reach 1. The reason for this has been illustrated in Section 4.3. The normalized acceleration/deceleration is shown in Fig. 29 and it stays within the safe zone during the whole simulation time.

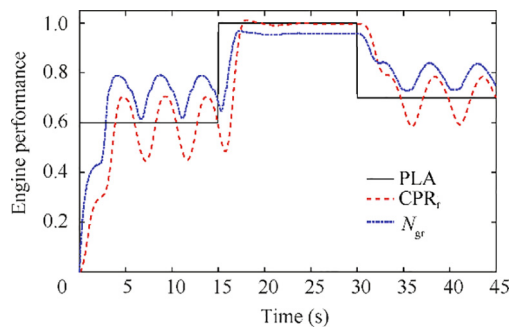
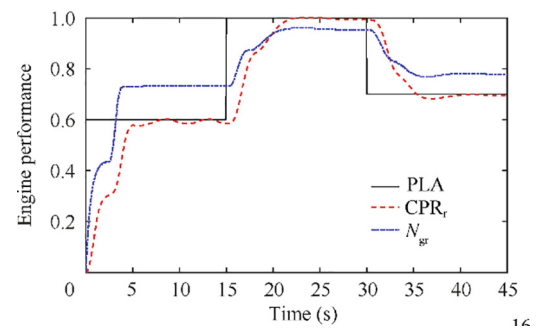
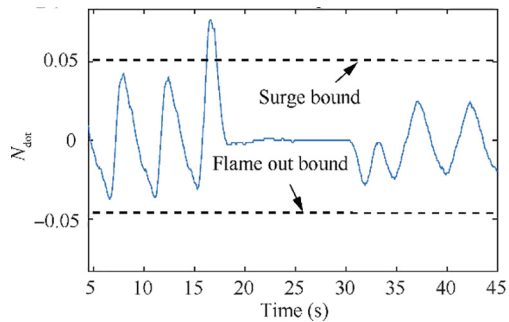
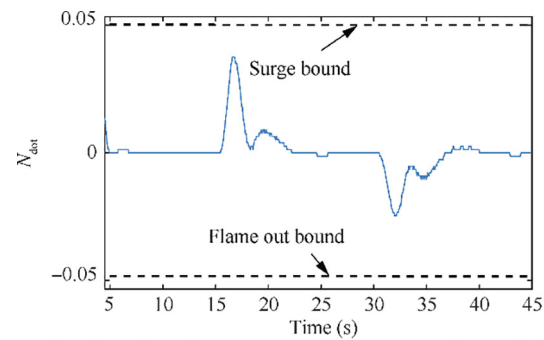
The comparisons between the engine performance in climb, TOC and cruise before and after optimization verifies the necessity of gains optimization, especially in the flight condition of high altitude and high Mach number.

Table 7 Optimized fuel controller parameters.

Parameter	K_{pla}	K_{Nmax}	K_{acc}	K_{dec}	Fitness	Optimization time
Optimized results	0.8327	1.1644	-0.0056	9.2603	0.7990	2490 s

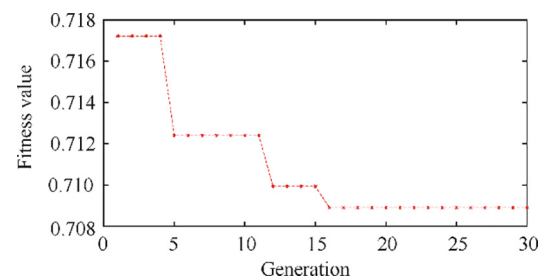
Table 8 Performance and penalty function values before and after optimization.

Parameter	RT	FC	P_1	P_2	P_3	P_4	P_5	P_6	Fitness
Initial	0.5947	0.5539	1.6522	1.2033	0.6209	0	0.4444	0.0618	1.2381
Optimized	0.9353	0.5349	0.1495	0.1570	0	0	0.0540	0.0229	0.7990

**Fig. 14** Tracking performance of CPR and N_{gr} with PLA before optimization.**Fig. 16** Tracking performance of CPR and N_{gr} with PLA after optimization.**Fig. 15** Derivative of engine rotor speed before the controller optimization.**Fig. 17** Derivative of engine rotor speed after controller optimization.

4.6. Approach ($H = 457.2$, $Ma = 0.233$)

The weather condition of approach is very similar to BOC. The main difference is that both the altitude and flight speed decrease during the approach condition while it is increase during BOC. The typical condition point of approach is $H = 457.2$, $Ma = 0.233$. Set this weather condition in the GTE controller model and apply LLGA on controller gains tuning, then the fitness value convergence and the standard deviation of the fitness value is shown in Fig. 30 and Fig. 31 respectively.

**Fig. 18** Static convergence of the minimum fitness value.

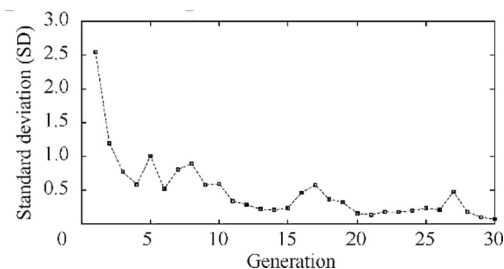


Fig. 19 Standard deviation of the fitness value at each generation.

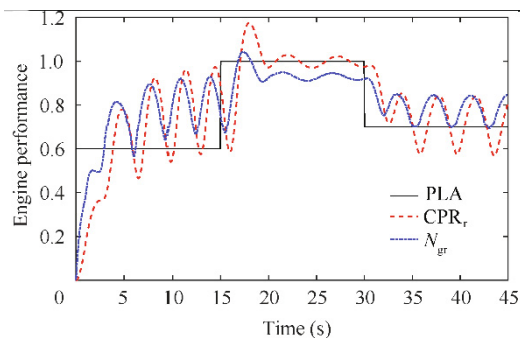


Fig. 20 Tracking performance of CPR and N_{gr} with PLA before optimization.

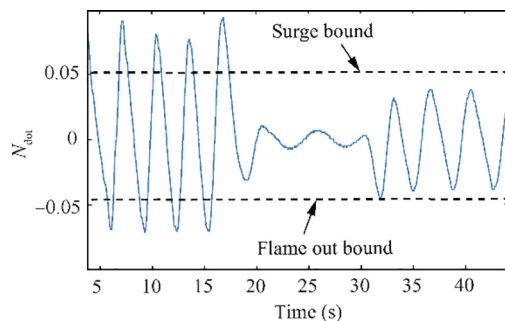


Fig. 21 Derivative of engine rotor speed before the controller optimization.

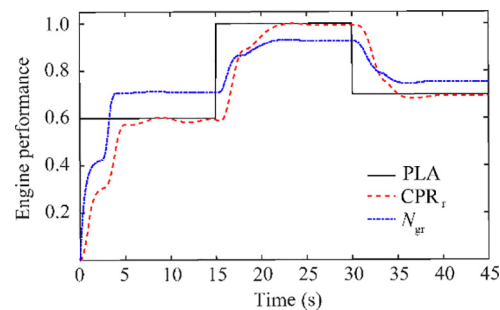


Fig. 22 Tracking performance of CPR and N_{gr} with PLA after optimization.

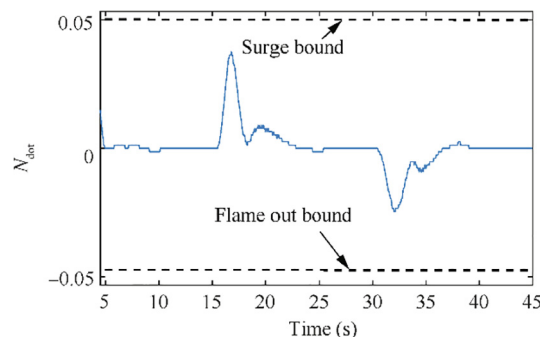


Fig. 23 Derivative of engine rotor speed after optimization.

The final optimization results are depicted in Table 13. Simulate the GTE controller model with the optimized gains and the initial gains respectively, then get the engine performance as shown in Table 14 and Fig. 32. The fitness value is reduced from 1.0780 to 1.0002 after optimization. The main improvements after optimization are the RT, fluctuation (P_1 , P_2) and the tracking error (P_3). The bad effect after optimization is that the maximum acceleration/deceleration value (P_5 , P_6) have some increase but does not exceed the limitation. The fuel consumption remains almost the same. Overall, the benefits

Table 9 Optimized controller parameters.

Parameter	K_{pla}	K_{Nmax}	K_{acc}	K_{dec}	Fitness	Optimization time
Optimized results	0.5391	2.5499	-0.0113	8.6438	0.7089	2488 s

Table 10 Performance and penalty function values before and after optimization.

Parameter	RT	FC	P_1	P_2	P_3	P_4	P_5	P_6	Fitness
Initial	0.5900	0.4038	3.4848	1.6902	8.7582	4.3137	0.9501	0.2887	3.7445
Optimized	0.9260	0.3484	0.1651	0.1802	0	0	0.0618	0.0229	0.7089

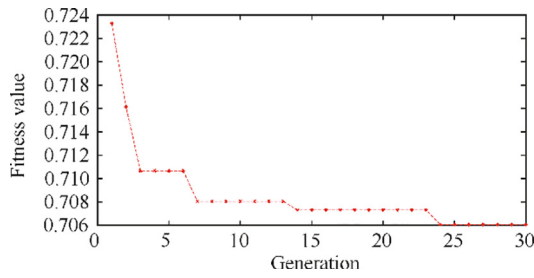


Fig. 24 Static convergence of the minimum fitness value.

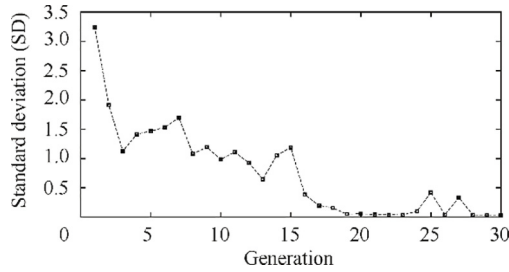


Fig. 25 Standard deviation of the fitness value at each generation.

brought in by the optimization greatly outweighs the side effects. In Fig. 32, the PLA, CPR_r and N_{gr} curves coincide at $PLA = 1$, the tracking error is negligible. This is because the rotational speed correction factor $\sqrt{\theta} = 1$ at approach condition. Therefore, both the values of CPR_r and N_{gr} will reach 1 when $PLA = 1$.

The normalized acceleration/deceleration is shown in Fig. 33. In the figure, both the N_{gr} derivative before and after optimization have not exceeded the safe bounds. Moreover, the optimized controller has used the safety margins to improve the engine performance.

5. Analysis of the control performance optimization effect in different flight conditions

Studying from the controller optimization results in all the flight conditions, it can be concluded that the control performance in each flight condition is improved in varying degrees by gains tuning through LLGA. The optimization effect is dependent on the value of $\sqrt{\theta}\delta$ and obeys the rules as below:

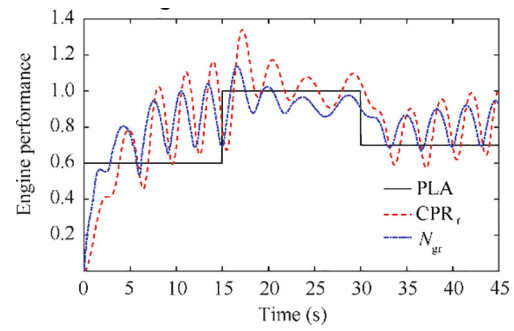


Fig. 26 Tracking performance of CPR and N_{gr} with PLA before optimization.

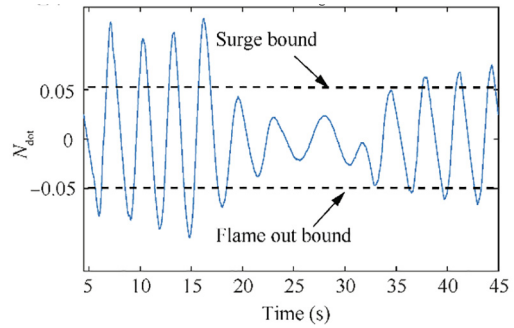


Fig. 27 Derivative of engine rotor speed before the controller optimization.

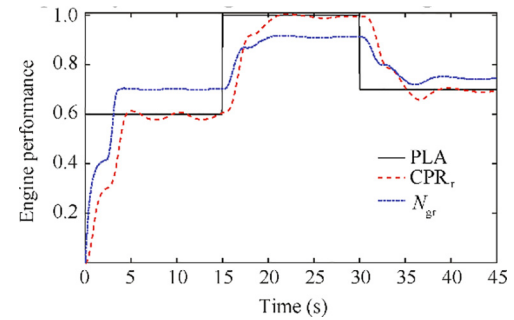


Fig. 28 Tracking performance of CPR and N_{gr} with PLA after optimization.

Table 11 Optimized fuel controller parameters.

Parameter	K_{pla}	K_{Nmax}	K_{acc}	K_{dec}	Fitness	Optimization time
Optimized results	0.5734	1.0783	-0.0388	2.7260	0.7061	2525 s

Table 12 Performance and penalty function values before and after optimization.

Parameter	RT	FC	P_1	P_2	P_3	P_4	P_5	P_6	Fitness
Initial	0.3567	0.3851	4.8890	2.6507	17.0153	13.7255	1.8060	1.1446	7.2427
Optimized	0.8560	0.2980	0.2405	0.2453	0.1961	0	0.0657	0.0268	0.7061

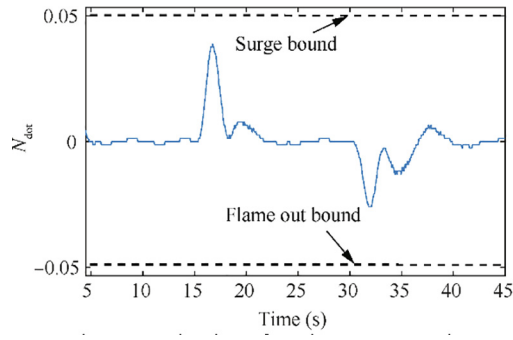


Fig. 29 Derivative of engine rotor speed.

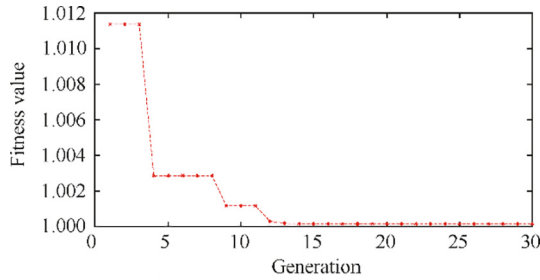


Fig. 30 Static convergence of the minimum fitness value.

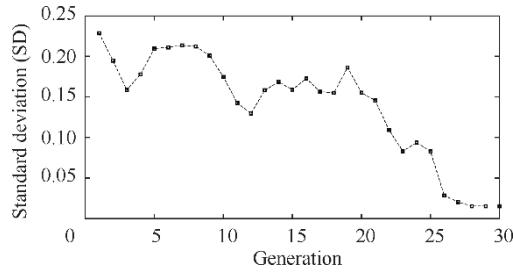


Fig. 31 Standard deviation of the fitness value at each generation.

- When $\sqrt{\theta\delta} \approx 1$, the control performance is improved after optimization, but the effect is not very remarkable;

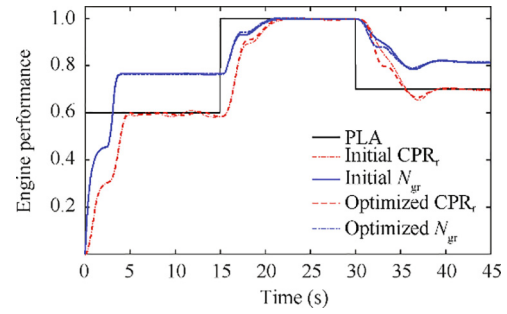


Fig. 32 Engine performance before and after optimization.

- When $\sqrt{\theta\delta} \ll 1$, the control performance with initial gains is too bad to be accepted, but it becomes very good after optimization;
- When $\sqrt{\theta\delta} \ll 1$ and with initial gains, the CPR and N_{gr} fluctuates dramatically and may deviate from the PLA command. The level of fluctuation and deviation is dependent on the value of $\sqrt{\theta\delta}$ and PLA settings. The smaller $\sqrt{\theta\delta}$ or PLA values will result in higher level of fluctuation and deviation of CPR and N_{gr} ;
- When $\sqrt{\theta\delta} \ll 1$, the standard deviation of the fitness value becomes much larger but converges fast.

5.1. Why the optimization effects are different?

Considering the fuel flow correction Eq. (9), the sensitivity of the rotational speed relative to the fuel flow is shown in Eq. (11). The equation shows the fact that the rotational speed in high conditions (weather conditions with low $\sqrt{\theta\delta}$) is more sensitive to the fuel flow change than in low conditions (weather conditions with high $\sqrt{\theta\delta}$). This leads to the difference in optimization effects for different flight conditions. Based on Eq. (11) and the N_{gr} -fuel flow schedule shown in Table 18, the working line of the engine in different flight conditions are depicted in Fig. 34. In this figure, the slope of the working line in altitude is $\sqrt{\theta\delta}$ times as in SLS condition.

$$\frac{dN_{gr}}{dW_{total}} = \frac{dN_{gr}}{d(\sqrt{\theta\delta} \cdot W_{total})} = \frac{1}{\sqrt{\theta\delta}} \cdot \frac{dN_{gr}}{dW_{total}} \quad (11)$$

Table 13 Optimized fuel controller parameters.

Parameter	K_{pla}	K_{Nmax}	K_{acc}	K_{dec}	Fitness	Optimization time
Optimized results	1.7280	4.0528	-0.0237	9.4364	1.0002	2504 s

Table 14 Performance and penalty function values before and after optimization.

Parameter	RT	FC	P_1	P_2	P_3	P_4	P_5	P_6	Fitness
Initial	0.9633	0.9593	0.1833	0.2438	0.1961	0	0.0735	0.0035	1.0780
Optimized	0.9073	0.9570	0.1267	0.1732	0	0	0.0774	0.0307	1.0002

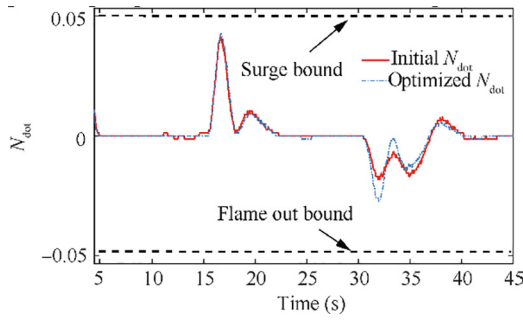


Fig. 33 Derivative of engine rotor speed before and after optimization.

5.2. Why fluctuation is more dramatical in high conditions and low PLA settings?

In high conditions, if the K_{pla} keeps constant, the same CPR error would induce the same fuel change and finally cause $1/(\sqrt{\theta}\delta)$ times N_{gr} change amount as in SLS condition. This is the reason why the controller with initial gains works well in low conditions while causes the fluctuation of CPR and N_{gr} in high conditions.

In low PLA settings, the N_{gr} is lower and the working line is flatter (see Fig. 34), which means the same fuel flow change will cause more rotational speed change. This is the reason why fluctuation is more dramatical at low PLA settings.

5.3. Why deviation is more serious in high conditions and low PLA settings?

In climb, as shown in Fig. 14, although the engine performance fluctuates, there is no obvious deviation of CPR from the PLA command. In TOC, as shown in Fig. 20, the CPR has a big deviation at PLA = 0.6. In cruise, as shown in Fig. 26, the CPR deviates at both PLA = 0.6 and PLA = 0.7 and the amplitude of deviation is larger than that of TOC. In order to explain this phenomenon, it is necessary to study the working process inside the Min-Max controller. As discussed in part I, the Min-Max selection rule is defined as below:

$$W_{ftrans} = \text{Min}(\text{Min}(\text{Max}(W_{fdec}, W_{fpla}), W_{face}), W_{fNmax}) \quad (12)$$

where W_{ftrans} is the fuel flow in transient control mode; W_{fpla} , W_{fdec} , W_{face} and W_{fNmax} are the fuel flows in the transient control loops of PLA loop, deceleration limitation loop, accelera-

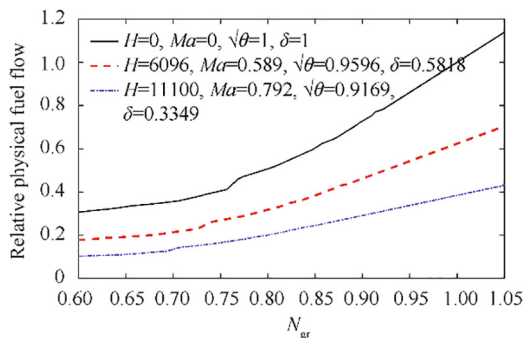


Fig. 34 Fuel-speed schedule in different flight conditions.

tion limitation loop and rotational speed limitation loop respectively.

In high conditions, the dramatical change in N_{gr} will increase the acceleration and deceleration, and this would make the W_{fdec} to be the winner in the Min-Max selection in most time. The dominance of deceleration loop in Min-Max selection would make the average W_{ftrans} to be higher than zero, which will finally cause the upward deviation of CPR and N_{gr} from the PLA command. Fig. 35 illustrates the fuel flow of different transient loops in Min-Max selection at cruise condition. Combining this figure with the tracking performance plot in cruise (Fig. 26), it can be found that W_{fdec} becomes the winner in the Min-Max selection in most time after the CPR reaches the PLA command for the first time (about the 5th second). The average W_{ftrans} during the time segments 5–15 s, 15–30 s and 35–45 s are 0.1557, -0.02658 and 0.03257 respectively. This means the deviation will first increases at PLA = 0.6 and then decreases at PLA = 1, and finally increases again at PLA = 0.7. The changing tendency of the deviation meets the simulation result in Fig. 26 very well.

In low PLA settings, the fluctuation is more serious as discussed in Section 5.2 and this will result in larger acceleration/deceleration and cause larger W_{fdec} which would finally result in higher W_{ftrans} . In addition, the N_{gr} is lower in low PLA settings and the working line is flatter (see Fig. 34) which means the same positive average W_{ftrans} fuel flow change will cause more rotational speed change. These two factors together aggravate the deviation of CPR and N_{gr} from the PLA command at low PLA settings.

5.4. A rough but effective estimation of optimal K_{pla} in different flight conditions to solve the fluctuation and deviation problems.

According to the analysis above, the deviation is caused by the too large W_{fdec} , and the large W_{fdec} is caused by the large fluctuation, while the large fluctuation is resulted from the too large K_{pla} relative to the sensitive N_{gr} in high conditions. Therefore, the fundamental cause of fluctuation and deviation is that the K_{pla} is too large in high conditions. As a result, the solution is reducing the K_{pla} to about $\sqrt{\theta}\delta$ times of the value in SLS condition ($1.7\sqrt{\theta}\delta$) so that the same amount of error between CPR and PLA command in different flight conditions will induce the same change in N_{gr} . This speculation is verified

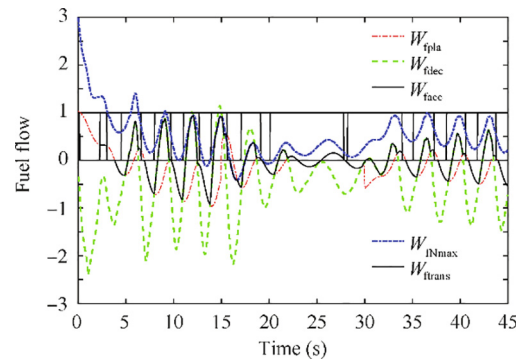


Fig. 35 Fuel flow of different transient loops in Min-Max selection at cruise condition.

by the value of $\sqrt{\theta\delta}$ times of initial K_{pla} and the optimized K_{pla} shown in Table 15 where the speculated K_{pla} is very approximately to the optimized K_{pla} in each flight condition.

In order to confirm the rationality of the speculated K_{pla} , the GTE controller with $K_{pla} = 1.7\sqrt{\theta\delta}$ and the other three gains remain the same as Table 2 will be simulated in the flight conditions of climb, TOC and cruise respectively. The engine performance in these three scenarios are depicted in Fig. 36, Fig. 37, and Fig. 38 respectively. In the three figures, it can be seen that the fluctuation and deviation are eliminated after replacing the initial K_{pla} as the speculated K_{pla} , which means K_{pla} is the most deterministic gain for control performance in high conditions. However, the appropriate K_{pla} value can only eliminates the fluctuation and deviation. If want to further improve the control performance, the gains optimization process is still indispensable. Table 16 shows the specific control performance which illustrates the optimization effects of LLGA relative to the controller with speculated K_{pla} . The results in this table show that the fitness values of optimized gains are a little lower than that of the speculated K_{pla} .

The correlation between K_{pla} and the flight condition above is based on the principle that the same amount of error between CPR and PLA command in different flight conditions should induce the same change in N_{gr} . The basement of the derivation is the fuel flow correction equation of turbojet engine which has been shown in Eq. (9). As the turboshaft engine has the same fuel flow correction equation as turbojet engine, so the correlation of K_{pla} is also applicable. If apply the correlation on turbofan engine, the non-dimensional temperature θ and pressure δ should be calculated in the section of the inlet of the compressor, i.e. the ratio between the total temperature/pressure of the outlet of the fan in flight condition and SLS condition.

5.5. Why the fitness standard deviation is much larger but converges faster in high conditions?

Comparing the simulation results from ground idle to cruise, it can be concluded that the fitness standard deviation varies greatly as the changing of flight conditions. The general trend is that the lower the $\sqrt{\theta\delta}$ value is, the larger the standard deviation is and also the faster it converges. The variation range and decreasing rate of the fitness standard deviation in different flight conditions are specified in Table 17. In this table, the standard deviation range of fitness value in the flight conditions of ground idle, take-off, approach and BOC are much smaller than that of climb, TOC and cruise. On the other hand, the generation needed to reduce the standard deviation by half for the former four flight conditions are much larger than that of the latter three flight conditions. In high conditions, for a given CPR error, the same K_{pla} change would induce the same fuel change and finally cause $1/(\sqrt{\theta\delta})$ times N_{gr} change amount as in SLS condition. As a result, the control performance is more sensitive to the change of K_{pla} and thus the gradient of the fitness value relative to the gains value is steeper in high conditions. This means that in the same gains searching domain, the variation range of the fitness value is larger in high conditions, which will cause the larger fitness standard deviation. However, this also means in high conditions the solution space for relative low fitness values is smaller and the local

optimizations are fewer. As a result, most of the individuals gather to the global optimization in a faster speed and the standard deviation converges faster than that in low conditions.

6. Parameter settings for flight mission simulation

The altitude and Mach number curves of the flight mission has been shown in Fig. 2 and the optimized gains for different flight conditions are specified in Appendix. The next important issue of flight mission simulation is to determine the PLA setting in each flight condition. For the turbojet engines, the PLA value is used to deliver the requirements for engine thrust from the aircraft in different flight conditions. Therefore, the PLA setting problem can be divided into two parts: the flight condition - thrust level regulation and the PLA- thrust regulation. As for the first part, a classical thrust level-flight condition schedule of turbojet engine is depicted in Fig. 39. As for the second part, the PLA- thrust regulation varies as the specific engines. In this paper, the engine controller model is based on the data of turbojet engine TRI 60-1. The PLA setting for each thrust level can be acquired by applying interpolation in thrust- N_{gr} schedule (Fig. 40), N_{gr} -fuel schedule (Table 18) and CPR-fuel schedule (Table 19) successively. After this step, all the simulation parameters are confirmed and depicted in Appendix. In addition, the Simulink model of the GTE controller for flight mission simulation is shown in Fig. 41.

7. Simulation results analysis

In order to verify the influences of the controller gains and weather conditions exerted on the engine performance, both variable and constant gain values will be applied to simulate the complete flight mission. In this section the flight mission will be simulated in three parameter configurations as shown in below:

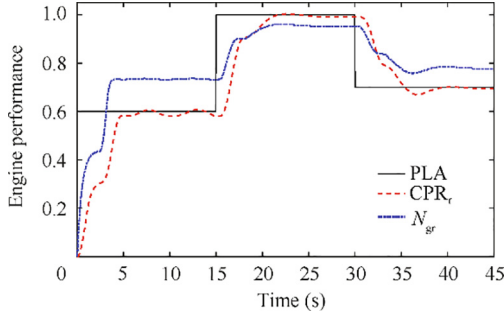
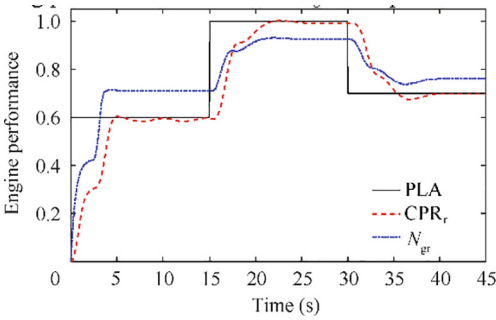
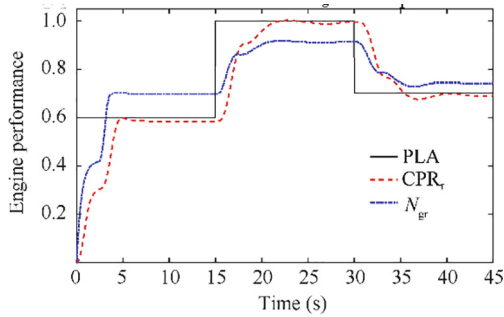
- Configuration 1: Initial gains and gradually changed altitude and Mach number;
- Configuration 2: Optimized gains and gradually changed altitude and Mach number;
- Configuration 3: Optimized gains and step changed altitude and Mach number.

7.1. Result of configuration 1

In this scenario, the controller with the initial gains will remain constant (shown in Table 2) and the flight conditions will change gradually as Fig. 2. The simulation result of this configuration is shown in Fig. 42. In this figure, the dramatical fluctuation and deviation of the CPR and N_{gr} begin from 20th minute and end at 92.5th minute, including the flight conditions of TOC, cruise, BOD and part of descent. This phenomenon for constant gains is caused by the small $\sqrt{\theta\delta}$ value which has been illustrated in Section 5. However, the separate flight condition simulation results in Section 4 have shown that the CPR and N_{gr} fluctuations with the initial controller are unstoppable in both climb and descent. Why the fluctuations in these two flight conditions are suppressed or

Table 15 Comparison between the speculated K_{pla} and the optimized K_{pla} .

Flight condition	Ground idle	Take-off	BOC	Climb	TOC	Cruise	Approach
$\sqrt{\theta}\delta$	1	1.04	1.061	0.5582	0.364	0.307	0.9843
Speculated $K_{pla}(1.7\sqrt{\theta}\delta)$	1.7	1.7680	1.8037	0.9489	0.6188	0.5219	1.6733
Optimized K_{pla}	1.7182	1.8307	1.8454	0.8327	0.5391	0.5734	1.7280

**Fig. 36** Tracking performance of CPR and N_{gr} with speculated K_{pla} in climb.**Fig. 37** Tracking performance of CPR and N_{gr} with speculated K_{pla} in TOC.**Fig. 38** Tracking performance of CPR and N_{gr} with speculated K_{pla} in cruise.

partly suppressed in flight mission simulation? The reason will be illustrated in follow.

It has been analyzed in Section 5 that smaller $\sqrt{\theta}\delta$, too large K_{pla} and lower PLA setting would aggravate the fluctuation and deviation of the engine performance. However, these three

factors could only reduce the robustness of the Min-Max controller and aggravate the fluctuation when some initial fluctuation is already generated. In principle, if there is no initial fluctuation, these factors will not generate fluctuation by themselves. In parameter configuration 1, the step change of PLA can be regarded as a sudden disturbance of the input which would trigger the initial fluctuation.

In order to analyse the causes for fluctuation and deviation in flight mission simulation with parameter configuration 1, the continuous changing of $\sqrt{\theta}\delta$ in the whole flight mission are shown in Fig. 43. In addition, the PLA setting, step change in PLA and $\sqrt{\theta}\delta$ values in the fluctuation flight conditions are specified in Table 20. K_{pla} values are not listed because their values are the same between separate flight condition simulation and flight mission simulation.

In Fig. 43, the value of $\sqrt{\theta}\delta$ decreases from 0.98 to 0.46 during the climb segment (15th–20th min). This means when the step change of PLA occurs at the beginning of climb segment, the $\sqrt{\theta}\delta$ value is large enough (0.98) to suppress the fluctuation. As a result, although the $\sqrt{\theta}\delta$ value is small enough (0.56, approximate to the representative $\sqrt{\theta}\delta$ value for climb segment) at 18th min, the fluctuation is still not generated because there is no initial fluctuation at this moment. At the beginning of TOC, the $\sqrt{\theta}\delta$ value is 0.46 and thereby the fluctuation of engine performance is triggered and aggravated immediately when the PLA setting has a small change. Fig. 44(a) shows the fuel flow of different transient loops in Min-Max selection at the beginning of TOC. At this moment, the dramatic fluctuation in N_{gr} leads to the increase of the acceleration and deceleration, and this makes the W_{fdec} to be the winner in the Min-Max selection in most time. Moreover, the dominance of deceleration loop in Min-Max selection makes the average W_{ftrans} to be higher than zero, which finally cause the upward deviation of CPR and N_{gr} from the PLA command (see Fig. 42). In this circumstance, the Min-Max controller cannot suppress the upward trend of fluctuation and deviation because it has entered the situation of positive feedback. In addition, the decrease of $\sqrt{\theta}\delta$ would aggravate this situation. As the increasing of fluctuation and deviation, the overspeed loop will finally be activated and become the winner of the Min-Max selection which makes the average W_{ftrans} to be zero again (see Fig. 44(b)). As a result, the fluctuation and deviation will no longer increase and remain in the high level during the cruise segment (see Fig. 42).

After the cruise condition, the fluctuation and deviation have a decrease in BOD as the increase of the $\sqrt{\theta}\delta$ value. The weather condition in descent segment is symmetrical with that in climb segment (see in Fig. 43), but their fluctuation characteristics are very different. This is also caused by the ini-

Table 16 Comparison of control performance with speculated K_{pla} and after optimization by LLGA.

Flight condition	Climb		TOC		Cruise	
Gains configuration	Speculated K_{pla}	Optimized gains	Speculated K_{pla}	Optimized gains	Speculated K_{pla}	Optimized gains
RT	0.9073	0.9353	0.912	0.926	0.9167	0.856
FC	0.54	0.5349	0.352	0.3484	0.2961	0.298
P_1	0.1907	0.1495	0.1898	0.1651	0.6275	0.2405
P_2	0.1814	0.157	0.1562	0.1802	0.2072	0.2453
P_3	0.1961	0	0.1743	0	0.1743	0.1961
P_4	0	0	0	0	0	0
P_5	0.0735	0.054	0.0696	0.0618	0.0657	0.0657
P_6	0.0268	0.0229	0.0268	0.0229	0.0268	0.0268
Fitness	0.8351	0.7990	0.7348	0.7089	0.7899	0.7061

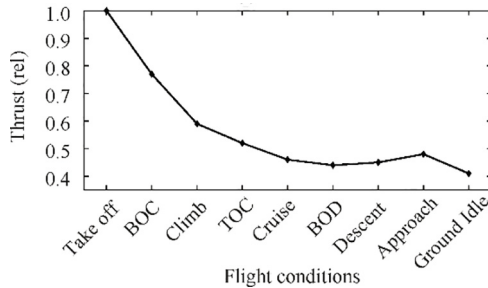
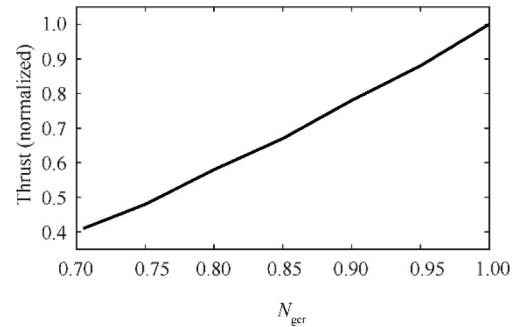
Table 17 Fitness standard deviation ranges and convergence speed in different flight conditions.

Parameter	Ground idle	Take-off	BOC	Climb	TOC	Cruise	Approach
$\sqrt{\theta} \cdot \delta$	1	1.04	1.061	0.5582	0.364	0.307	0.9843
Range of standard deviation	0–0.25	0–0.28	0–0.28	0–0.7	0–2.5	0–3.5	0–2.5
Generation of standard deviation reduced by half	25	25	> 40	2	2	3	22

Table 18 Fuel schedule between N_{gr} and fuel flow.

N_{gr}	0	0.6100	0.6367	0.6550	0.6833	0.7057	0.7293	0.7333	0.7567	0.7683	0.7733
$W_{fc}(\text{kg/h})$	0	139.4	144.7	149.9	155.2	160.4	171.0	173.6	184.1	205.1	210.4
N_{gr}	0.8033	0.8133	0.8430	0.8570	0.8707	0.8903	0.8980	0.9097	0.9137	0.9217	1.0
$W_{fc}(\text{kg/h})$	228.8	236.7	263.0	278.8	289.3	313.0	323.5	336.6	344.5	349.8	447.1

Notes: N_{gr} —relative corrected rotational speed; W_{fc} —corrected fuel flow;

**Fig. 39** Thrust setting of a turbojet engine during a flight cycle.**Fig. 40** Thrust-speed curve of TRI 60-1.

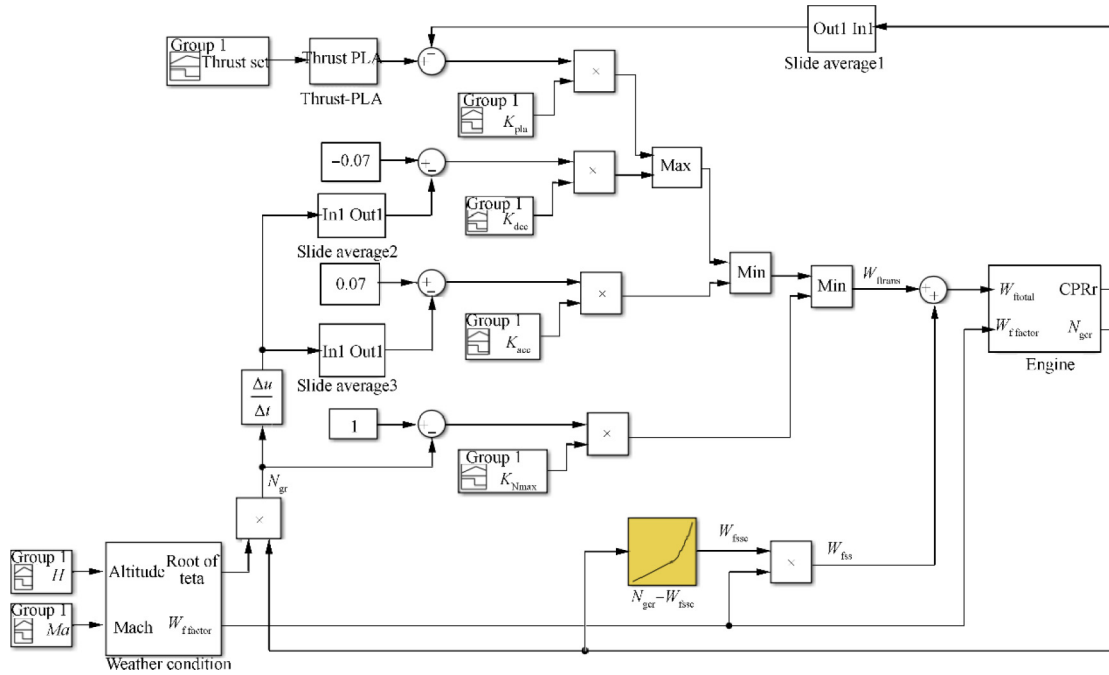
tial fluctuation. At the beginning of descent segment, the $\sqrt{\theta}\delta$ value is 0.46 and there already exists some big fluctuation at this moment. As a result, the fluctuation can be continued although the step change is very tiny (0.005). However, when the $\sqrt{\theta}\delta$ value increases to about 0.68 at 92.5th min, the Min-Max controller becomes robust enough to suppress the fluctuation and deviation. As a result, the PLA loop will become the winner of the Min-Max selection again (see Fig. 44(c)). Therefore, there is no fluctuation in the second half part of the descent segment.

Combining Fig. 42 and Fig. 43, it can be concluded that the robustness of the Min-Max controller becomes very weak when $\sqrt{\theta}\delta$ is smaller than 0.68 if the gains remain constant. In this circumstance, the fluctuation and deviation of CPR and N_{gr} can be easily triggered by some sudden disturbance such as step change in PLA. In addition, the initial fluctuation will be aggravated and leads to upward deviation as the decrease of $\sqrt{\theta}\delta$ while the existing fluctuation will decay as the increase of $\sqrt{\theta}\delta$.

Table 19 Fuel schedule between CPR_r and fuel flow.

CPR_r	0.2703	0.5792	0.5881	0.6108	0.6811	0.7108	0.7270	0.7459	0.7595	0.7838	0.8108	0.8297	0.8541	0.8649	1.0
W_{fc} (kg/h)	0 ^a	194.6	199.9	205.1	226.2	247.2	255.1	265.6	278.8	289.3	313.0	323.5	336.6	344.5	447.1

Notes: W_{fc} —corrected fuel flow; a—when fuel flow is zero, $CPR = 1$.

**Fig. 41** Simulink model of engine controller for flight mission simulation.

7.2. Result of configuration 2

The parameter settings and weather condition of this configuration are shown in the Appendix A and Fig. 2. Fig. 45 is the simulation result of this scenario. In the figure, the tracking performance of CPR and N_{gr} with PLA is very good during the whole flight mission. The tracking error is negligible and the overshoot/undershoot is very small. This verifies the fact that the robustness of the Min-Max controller in high conditions has been enhanced with the optimized controller gains (mainly is the K_{pla}). As a result, the control performance is significantly improved after optimization.

7.3. Result of configuration 3

In this scenario, the altitude and Mach number keep constant in a flight condition. Therefore, there is a step change between two flight conditions (see Fig. 46). Although in practice it is impossible for altitude and Mach number to have a sudden change, the simulation with this configuration can illustrate the influence of the dramatically changed flight condition exerts on the control performance. Fig. 47 is the simulation result of this scenario. The tracking performance

of CPR and N_{gr} with PLA is very good during the whole flight mission except the big overshoot/undershoot at the joint of two flight conditions. The simulation results show that the sudden change in weather condition would cause great overshoot or even overspeed. However, with the optimized GTE controller whose robustness has been enhanced after optimization, the overshoot or overspeed will be eliminated in several seconds.

8. Comparison between the control performance with different parameter configurations

In order to compare the control performance with different parameter configurations, the quantitative simulation results are depicted in Table 21 and the specific control performance of each flight condition segment of the three parameter configurations are specified in Table 22, Table 23, and Table 24 respectively.

In Table 21, the flight mission simulation with parameter configuration 2 has the least response time, overshoot, tracking error and acceleration. However, almost all the data for the performance indices and penalty items of configuration 1 are too bad to be accepted. The main reason for this is that the

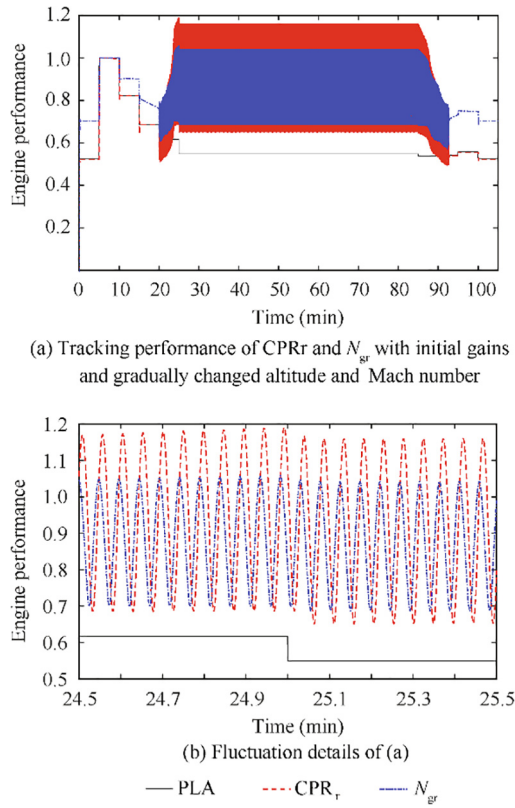


Fig. 42 Tracking performance of CPR_r and N_{gr} with initial gains and gradually changed altitude and Mach number.

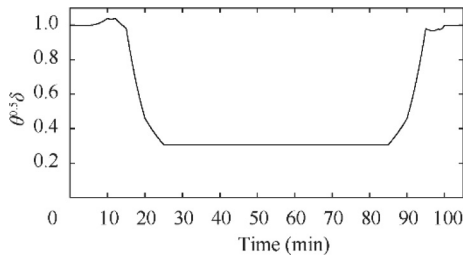


Fig. 43 Change of $\sqrt{\theta\delta}$ during the whole flight mission.

constant gain values are not suitable for both low conditions and high conditions which has been discussed in Sections 4 and 5. In addition, as the CPR cannot achieve the value of

PLA during the cruise and BOD segments because of deviation in parameter configuration 1, the response time of these two flight condition segments are very long (see Table 22). This makes the total response time of parameter configuration 1 is much longer than that of other two configurations. The comparison between configuration 1 and configuration 2 shows that the control performance has been greatly improved after controller optimization.

As for the configuration 3, it can be seen that the fuel consumption is fewer than configuration 2 and CPR tracking error is equal to configuration 2 while other indices are much worse than configuration 2. This means the steep change in altitude and Mach number could get the benefits of fuel saving although it may induce the safety problems. This verifies the fact that in order to save fuel, the aircraft should accelerate and climb to the stratosphere as soon as possible under the premise of ensuring safety.

It can be seen from the Table 23 and Table 24 that the response times of BOD, descent and approach condition are zero. The reason for zero response time is that the definition of reaching a flight condition is that the difference between CPR and PLA setting is less than 0.15. Moreover, the PLA settings for cruise, BOD, descent and approach are quite approximate to each other. This means there exists some CPR value that can meet the requirement for the four flight conditions at the same time and thereby the response time would be zero.

9. Conclusion

In part I, the methodology of using the LLGA based on mGA to optimize the GTE controller gains is illustrated and the LLGA method is applied in gains tuning in runway from ground idle to takeoff condition. In this part, the LLGA method is extended to the controller optimization problems in other flight conditions of a complete flight mission. For this purpose, firstly the weather condition is considered in the GTE controller model to correct the control parameters under SLS. Then a typical flight mission is defined and separated into ten segments. For the sake of simplicity, one representative point is selected from each segment as the characteristic weather condition for optimization. After that, the LLGA method is used to optimize the controller gains in each flight condition. The simulation results show that the control performance of each flight condition is improved in different extent after optimization. The optimization effect is dependent on the value of $\sqrt{\theta\delta}$. In high conditions, the controller with initial gains will cause

Table 20 influence factors of fluctuation for fluctuating flight conditions.

Flight condition		Climb	TOC	Cruise	BOD	Descent	
Separate flight condition simulation	PLA	0.6	0.6	0.6	0.6	0.6	
	ΔPLA	0.6	0.6	0.6	0.6	0.6	
	$\sqrt{\theta\delta}$	0.5582	0.364	0.307	0.364	0.5582	
	Fluctuation	Yes	Yes	Yes	Yes	Yes	
Flight mission simulation	PLA	0.687	0.617	0.549	0.538	0.543	
	ΔPLA	-0.145	-0.07	-0.068	-0.011	0.005	
	$\sqrt{\theta\delta}$	0.98-0.46	0.46-0.31	0.31	0.31-0.46	0.46-0.68	0.68-0.98
	Fluctuation	No	Yes	Yes	Yes	Yes	No

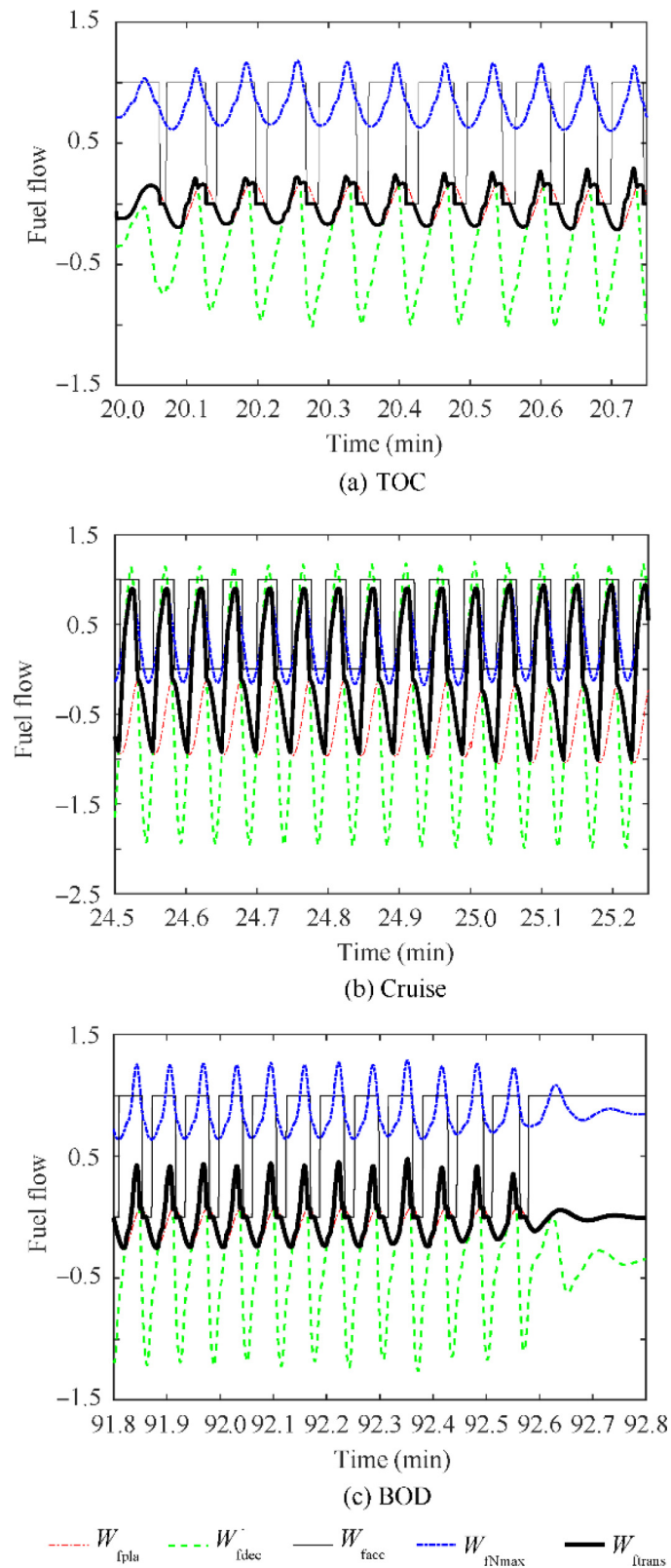


Fig. 44 Fuel flow of different transient loops in Min-Max selection.

deviation and fluctuation of CPR relative to the PLA command. The fundamental reason for deviation and fluctuation is that the value of $\sqrt{\theta}\delta$ is too low and thus the rotational

speed is more sensitive to the fuel flow. The solution to eliminate the deviation and fluctuation is to set the value of K_{pla} in high conditions as $\sqrt{\theta}\delta$ times of K_{pla} in SLS condition.

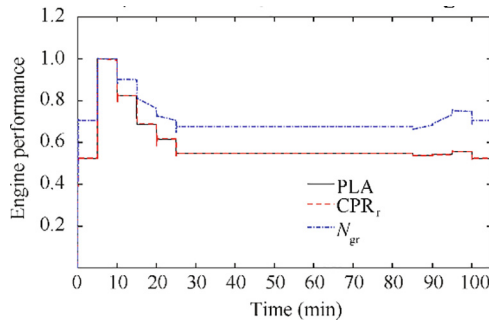


Fig. 45 Tracking performance of CPR_r and N_{gr} with optimized gains and gradually changed altitude and Mach number.

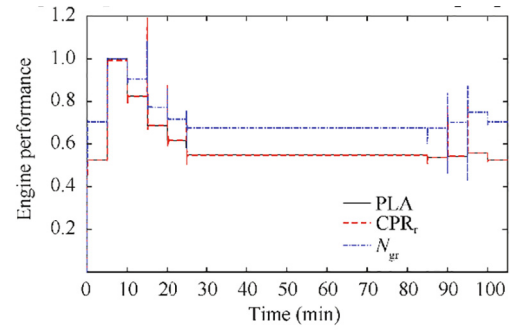


Fig. 47 Tracking performance of CPR_r and N_{gr} with optimized gains and step changed altitude and Mach number.

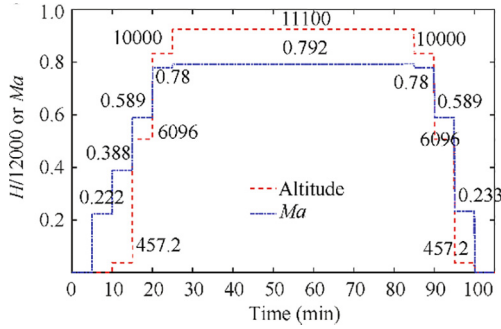


Fig. 46 Step changed altitude and Mach number during flight mission.

As the aircraft flying in the sky, the altitude and Mach number vary simultaneously. This leads to the changing of $\sqrt{\theta\delta}$ which directly influences the sensitivity of N_{gr} relative to the change of fuel flow. As a result, the robustness of the GTE controller with constant initial gains will be weakened in the flight conditions with lower $\sqrt{\theta\delta}$ value such as climb, TOC, cruise, etc. Therefore, the GTE controller based on the

Min-Max selection with constant initial gains is not suitable for all the flight conditions during the whole flight mission. There are two preconditions to generate the fluctuation of the CPR and N_{gr} , i.e. small $\sqrt{\theta\delta}$ value and initial fluctuation. In high conditions with $\sqrt{\theta\delta}$ smaller than 0.68, the robustness of the GTE controller with initial gains is too weak to suppress the initial fluctuation of CPR and N_{gr} . In this circumstance, a small disturbance caused by step change of PLA would lead to the great fluctuation and then make the deceleration loop to be the winner in the Min-Max selection. As a result, the average transient fuel flow would be larger than zero which finally leads to the upward deviation of CPR and N_{gr} relative to the PLA command. The growing fluctuation and deviation reach their limits at the beginning of cruise segment because the over-speed loop is activated. The robustness of the GTE controller is strengthened after the gains optimization for different flight conditions through LLGA. As a result, the fluctuation and deviation can be eliminated at the initial phase. The engine performance improved by controller optimization is mainly manifested in the transient state and the high conditions. In other steady states, the optimization effect is not very obvious. In addition, the simulation results with the step changed weather

Table 21 Control performance of the flight mission with different parameter configurations.

Configuration	Response time (s)	Fuel consumption (kg)	Max overshoot	Max error	Max over-speed	Max N_{dot}	Min N_{dot}
Configuration 1	3857.84	272.08	0.618	0.618	0.058	0.327	-0.309
Configuration 2	28.84	195.08	0.034	0.008	0.004	0.147	-0.053
Configuration 3	31.53	192.16	0.235	0.008	0.084	0.355	-0.272

Table 22 Specific control performance of the flight mission with configuration 1.

Parameter	GI	TO	BOC	Climb	TOC	Cruise	BOD	Descent	Approach	GI
Response time(s)	6.55	6.16	3.70	2.97	1.57	3599.96	231.73	2.02	0.95	2.24
Fuel consumption(kg)	13.31	37.42	27.25	13.39	9.15	122.53	10.23	10.70	14.73	13.36
Max overshoot	0.015	0.014	0.020	0.045	0.114	0.618	0.374	0.293	0.015	0.014
Max error	0	0.008	0	0.001	0.575	0.618	0.349	0.232	0	0
Max over speed	0	0	0	0	0.058	0.046	0.039	0	0	0
Max N_{dot}	0.118	0.147	0.005	0.023	0.327	0.327	0.325	0.222	0.012	0.011
Min N_{dot}	-0.004	0	-0.045	-0.051	-0.307	-0.309	-0.304	-0.210	-0.003	-0.024

Table 23 Specific control performance of the flight mission with configuration 2.

Parameter	GI	TO	BOC	Climb	TOC	Cruise	BOD	Descent	Approach	GI
Response time(s)	6.33	5.54	3.19	5.88	2.41	2.07	0	0	1.23	2.18
Fuel consumption(kg)	13.31	37.45	27.25	13.47	6.52	53.81	5.31	9.89	14.73	13.36
Max overshoot	0.015	0.015	0.030	0.015	0.034	0.022	0.010	0.006	0.015	0.015
Max error	0	0.008	0	0.003	0.001	0	0.001	0.002	0	0
Max over speed	0	0.004	0	0	0	0	0	0	0	0
Max $N_{\dot{}}_{dot}$	0.118	0.147	0.009	0	0.008	0.016	0.002	0.004	0.013	0.011
Min $N_{\dot{}}_{dot}$	-0.004	-0.003	-0.053	-0.025	-0.026	-0.038	-0.007	-0.001	-0.003	-0.025

Table 24 Specific control performance of flight mission with configuration 3.

Parameter	GI	TO	BOC	Climb	TOC	Cruise	BOD	Descent	Approach	GI
Response time(s)	6.33	5.71	3.08	8.12	3.70	2.58	0	0	0	2.02
Fuel consumption(kg)	13.31	38.08	28.33	10.89	6.29	53.84	5.10	8.02	14.91	13.36
Max overshoot	0.015	0.015	0.031	0.019	0.031	0.045	0.032	0.235	0.220	0.014
Max error	0	0.008	0	0	0.002	0	0	0	0	0
Max over speed	0	0.005	0	0.084	0	0	0	0	0	0
Max $N_{\dot{}}_{dot}$	0.118	0.163	0.010	0.178	0.087	0.119	0.041	0.308	0.355	0.010
Min $N_{\dot{}}_{dot}$	-0.004	-0.024	-0.051	-0.093	-0.080	-0.117	-0.072	-0.210	-0.272	-0.022

condition show that a relative high altitude and Mach number is beneficial for fuel saving. In practice, the weather condition varies continuously during the flight. As a result, if the controller gains could be optimized simultaneously according to the current condition, then the engine performance is expected to be further improved. This would become an important research point in the next stage.

Declaration of Competing Interest

The authors declare that they have no known competing financial interests or personal relationships that could have appeared to influence the work reported in this paper.

Acknowledgements

The authors are grateful to the anonymous reviewers for their critical and constructive review of the manuscript. Great appreciation should also be delivered to Aero-engine Corporation of China (AECC), China Scholarship Council (CSC) and China Aviation Powerplant Institute (CAPI) for offering the precious opportunity to LIU Yinfeng to study in Cranfield University.

Appendix A

See [Table A1](#) and [Table A2](#)

Table A1 Parameter settings during the Flight mission.

Parameter	Time segment (min)									
	0–5	6–10	11–15	16–20	21–25	26–85	86–90	91–95	96–100	101–105
Flight condition	GI	TO	BOC	Climb	TOC	Cruise	BOD	Descent	Approach	GI
FN	0.41	1	0.77	0.59	0.52	0.46	0.44	0.45	0.48	0.41
PLA	0.525	1	0.823	0.687	0.617	0.549	0.538	0.543	0.558	0.525
K_{pla}	1.7182	1.8307	1.8454	0.8327	0.5391	0.5734	0.5391	0.8327	1.7280	1.7182
K_{Nmax}	4.2329	4.9295	4.9452	1.1644	2.5499	1.0783	2.5499	1.1644	4.0528	4.2329
K_{acc}	-0.0473	-0.0302	-0.0496	-0.0056	-0.0113	-0.0388	-0.0113	-0.0056	-0.0237	-0.0473
K_{dec}	8.5910	8.2035	7.9746	9.2603	8.6438	2.7260	8.6438	9.2603	9.4364	8.5910
Altitude (m)	0	0	0–1524	1524–7620	7620–11,100	11,100	11100–7620	7620–1524	1524–0	0
Time segment (min)	0–5	6–10	11–12	13–22	23–25	26–85	86–88	89–95	96–98	99–100
Mach	0	0–0.222	0.222–0.388	0.388–0.7	0.7–0.792	0.792	0.792–0.7	0.7–0.48	0.48–0.233	0.233–0

Table A2 Performance and penalty items for different flight conditions before and after optimization.

Flight condition		RT	FC	P_1	P_2	P_3	P_4	P_5	P_6	Fitness	Optimization time
Ground idle	Initial	0.9773	0.9735	0.1852	0.2333	0.1961	0	0.0735	0.0035	1.0907	
	Optimized	0.9120	0.9730	0.0261	0.1808	0	0	0.0696	0.0268	0.9931	2523 s
Take-off	Initial	1.0567	1.0054	0.1775	0.1961	0.5882	0	0.0696	0	1.2029	–
	Optimized	0.9027	1.0073	0.1024	0.1945	0.1961	0	0.0813	0.0229	1.0545	2498 s
BOC	Initial	1.6993	1.0173	0.1719	0.1886	0.9804	0	0.0696	0.0035	1.5940	–
	Optimized	0.9167	1.0222	0.0504	0.1780	0.5882	0	0.0813	0.0229	1.1229	3321 s
Climb	Initial	0.5947	0.5539	1.6522	1.2033	0.6209	0	0.4444	0.0618	1.2381	–
	Optimized	0.9353	0.5349	0.1495	0.1570	0	0	0.0540	0.0229	0.7990	2490 s
TOC	Initial	0.5900	0.4038	3.4848	1.6902	8.7582	4.3137	0.9501	0.2887	3.7445	–
	Optimized	0.9260	0.3484	0.1651	0.1802	0	0	0.0618	0.0229	0.7089	2488 s
Cruise	Initial	0.3567	0.3851	4.8890	2.6507	17.0153	13.7255	1.8060	1.1446	7.2427	–
	Optimized	0.8560	0.2980	0.2405	0.2453	0.1961	0	0.0657	0.0268	0.7061	2525 s
Approach	Initial	0.9633	0.9593	0.1833	0.2438	0.1961	0	0.0735	0.0035	1.0780	–
	Optimized	0.9073	0.9570	0.1267	0.1732	0	0	0.0774	0.0307	1.0002	2504 s

References

- Mattingly JD. *Elements of propulsion: Gas turbines and rockets*. Reston: AIAA Education Series; 2006. p. 441–4.
- Jafari S, Nikolaidis T. Meta-heuristic global optimization algorithms for aircraft engines modelling and controller design: A review, research challenges, and exploring the future. *Prog Aerosp Sci* 2019;**104**:40–53.
- Montazeri-Gh M, Jafari S, Ilkhani MR. Application of particle swarm optimization in gas turbine engine fuel controller gain tuning. *Eng Optim* 2012;**44**(2):225–40.
- Jafari S, Majidi PM, Sohrabi S, et al. Advanced modeling and control of 5 MW wind turbine using global optimization algorithms. *Wind Eng* 2018;**43**(5):1–18.
- Jafari S, Montazeri-Gh M. Evolutionary optimization for gain tuning of jet engine Min-Max fuel controller. *J Propul Power* 2011;**27**(5):1015–23.
- Jafari S, Nikolaidis T. Turbojet engine industrial Min-Max controller performance improvement using fuzzy norms. *Electronics* 2018;**7**(11):314.
- Chang X, Yang G. Nonfragile H_∞ filter design for T-S fuzzy systems in standard form. *IEEE Trans Ind Electron* 2014;**61**(7):3448–58.
- Zhao X, Wang X, Ma L, et al. Fuzzy approximation based asymptotic tracking control for a class of uncertain switched nonlinear systems. *IEEE Trans Fuzzy Syst* 2020;**28**(4):632–44.
- Zhang JX, Yang GH. Supervisory switching-based prescribed performance control of unknown nonlinear systems against actuator failures. *Int J Robust Nonlinear Control* 2020;**30**(6):2367–85.
- Lu AY, Yang GH. Switched projected gradient descent algorithms for secure state estimation under sparse sensor attacks. *Automatica* 2019;**103**:503–14.
- Zhang L, Yang GH. Low-computation adaptive fuzzy tracking control for nonlinear systems via switching-type adaptive laws. *IEEE Trans Fuzzy Syst* 2019;**27**(10):1931–42.
- Yang D, Huang C, Zong G. Finite-time H_∞ bumpless transfer control for switched systems: A state-dependent switching approach. *Int J Robust Nonlinear Control* 2020;**30**(4):1417–30.
- Huo X, Ma L, Zhao X, et al. Event-triggered adaptive fuzzy output feedback control of MIMO switched nonlinear systems with average dwell time. *Appl Math Comput* 2020;**365**:1–16.
- Lu AY, Yang GH. Secure switched observers for cyber-physical systems under sparse sensor attacks: A set cover approach. *IEEE Trans Autom Control* 2019;**64**(9):3949–55.
- Hou L, Zhao X, Sun H, et al. l_2 – l_∞ filtering of discrete-time switched systems via admissible edge-dependent switching signals. *Syst Control Lett* 2018;**113**:17–26.
- Ma L, Sun H, Zong G. Feedback passification of switched stochastic time-delay systems with multiple disturbances via DOBC. *Int J Robust Nonlinear Control* 2020;**30**(4):1696–718.
- Lin J, Zhao X, Xiao M, et al. Stabilization of discrete-time switched singular systems with state, output and switching delays. *J Franklin Inst* 2019;**356**(4):2060–89.
- Yang J, Zhao X, Bu X, et al. Stabilization of switched linear systems via admissible edge-dependent switching signals. *Nonlinear Anal Hybrid Syst* 2018;**29**:100–9.
- Li X, Wang R, Zhao X. Stability of discrete-time systems with time-varying delay based on switching technique. *J Franklin Inst* 2018;**355**(13):6026–44.
- Du S, Qiao J, Zhao X, et al. Stability and L_1 -gain analysis for switched positive T-S fuzzy systems under asynchronous switching. *J Franklin Inst* 2018;**355**(13):5912–27.
- Hou L, Zhang M, Zhao X, et al. Stability of discrete-time switched systems with admissible edge-dependent switching signals. *Int J Syst Sci* 2018;**49**(5):974–83.

2020-08-15

Advanced optimization of gas turbine aero-engine transient performance using linkage-learning genetic algorithm: Part I, Optimization in flight controller gains correlation development

Liu, Yinfeng

Elsevier

Liu Y, Jafari S, Nikolaidis T. (2021) Advanced optimization of gas turbine aero-engine transient performance using linkage-learning genetic algorithm: Part II: Optimization in flight mission and controller gains correlation development. Chinese Journal of Aeronautics, Volume 34, Issue 4, April 2021, pp. 568-588

<https://doi.org/10.1016/j.cja.2020.07.037>

Downloaded from Cranfield Library Services E-Repository